https://doi.org/10.5194/gmd-2019-281
Preprint. Discussion started: 30 October 2019

Geoscientific Model Development
Discussions
Open Access

Implementation of Yale Interactive terrestrial Biosphere model version 1.0 into GEOS-Chem version 12.0.0: a tool for biosphere-chemistry interactions

Yadong Lei[1,2], Xu Yue[3], Hong Liao[3], Cheng Gong[2,4], Lin Zhang[5]

[1]Climate Change Research Center, Institute of Atmospheric Physics, Chinese Academy of Sciences, Beijing 100029, China

[2]University of Chinese Academy of Sciences, Beijing, China

[3]Jiangsu Key Laboratory of Atmospheric Environment Monitoring and Pollution Control, Collaborative Innovation Center of Atmospheric Environment and Equipment Technology, School of Environmental Science and Engineering, Nanjing University of Information Science & Technology (NUIST), Nanjing, 210044, China

[4]State Key Laboratory of Atmospheric Boundary Layer Physics and Atmospheric Chemistry (LAPC), Institute of Atmospheric Physics, Chinese Academy of Sciences, Beijing, 100029, China

[5]Laboratory for Climate and Ocean–Atmosphere Studies, Department of Atmospheric and Oceanic Sciences, School of Physics, Peking University, Beijing 100871, China

Correspondence to: Xu Yue (yuexu@nuist.edu.cn)

Abstract: The terrestrial biosphere and atmospheric chemistry interact through multiple feedbacks, but the models of vegetation and chemistry are developed separately. In this study, the Yale Interactive terrestrial Biosphere (YIBs) model, a dynamic vegetation model with biogeochemical processes, is implemented into the Chemical Transport Model GEOS-Chem version 12.0.0. Within the GC-YIBs framework, leaf area index (LAI) and canopy stomatal conductance dynamically predicted by YIBs are used for dry deposition calculation in GEOS-Chem. In turn, the simulated surface ozone (O_3) by GEOS-Chem affect plant photosynthesis and biophysics in YIBs. The updated stomatal conductance and LAI improve the simulated daytime O_3 dry deposition velocity for major tree species. Compared with the GEOS-Chem model, the model-to-observation correlation for dry deposition velocities increases from 0.76 to 0.85 while the normalized mean error decreases from 35% to 27% using the GC-YIBs model. Furthermore, we quantify O_3 vegetation damaging effects and find a global reduction of annual gross primary productivity by 2-5%, with regional extremes of 11–15% in the eastern U.S. and eastern China. The online GC-YIBs model provides a useful tool for discerning the complex feedbacks between atmospheric chemistry and terrestrial biosphere under global change.

Keywords: GC-YIBs model, biosphere-chemistry interactions, dry deposition, ozone vegetation damage

https://doi.org/10.5194/gmd-2019-281
Preprint. Discussion started: 30 October 2019

Geoscientific Model Development
Discussions
Open Access
EGU

1 Introduction

The terrestrial biosphere interacts with atmospheric chemistry through the exchanges of trace gases, water, and energy (Green et al., 2017; Hungate and Koch, 2015). Emissions from terrestrial biosphere, such as biogenic volatile organic compounds (BVOCs) and nitrogen oxides (NO_x) affect the formation of air pollutants and chemical radicals in the atmosphere (Kleinman, 1994; Li et al., 2019). Globally, terrestrial biosphere emits ~1100 Tg (1 Tg = 10^{12} g) BVOC annually, which is approximately ten times more than the total amount of VOC emitted worldwide from anthropogenic sources including fossil fuel combustion and industrial activities (Carslaw et al., 2010). Meanwhile, the biosphere acts as a major sink through dry deposition of air pollutants, such as surface ozone (O_3) and aerosols (Fowler et al., 2009; Park et al., 2014; Petroff, 2005). Dry deposition accounts for ~25% of the total O_3 removed from the troposphere (Lelieveld and Dentener, 2000).

In turn, atmospheric chemistry can also affect the terrestrial biosphere (McGrath et al., 2015; Schiferl and Heald, 2018; Yue and Unger, 2018). Surface O_3 has a negative impact on plant photosynthesis and crop yields by reducing gas-exchange and inducing phytotoxic damages on plant tissues (Van Dingenen et al., 2009; Wilkinson et al., 2012; Yue and Unger, 2014). Unlike O_3, the increase of aerosols in the atmosphere is beneficial to vegetation (Mahowald, 2011; Schiferl and Heald, 2018). The aerosol-induced enhancement in diffuse light results in more radiation reaching surface from all directions than solely from above. As a result, leaves in the shade or

https://doi.org/10.5194/gmd-2019-281
Preprint. Discussion started: 30 October 2019

at the bottom can receive more radiation and are able to assimilate more CO_2 through photosynthesis, leading to an increase of canopy productivity (Mercado et al., 2009; Yue and Unger, 2018).

Models are essential tools to understand and quantify the interactions between terrestrial biosphere and atmospheric chemistry at the global and/or regional scales. Many studies have performed multiple global simulations with climate-chemistry-biosphere models to quantify the effects of air pollutants on terrestrial biosphere (Mercado et al., 2009; Oliver et al., 2018; Schiferl and Heald, 2018; Yue and Unger, 2015). In contrast, very few studies have quantified the O_3-induced biogeochemical and meteorological feedbacks to air pollution concentrations (Sadiq et al., 2017; Zhou et al., 2018). Although considerable efforts have been made, uncertainties in biosphere-chemistry interactions remain large because their two-way coupling is not adequately represented in current generation of terrestrial biosphere models or global chemistry models. Global terrestrial biosphere models usually use prescribed O_3 and aerosol concentrations (Lombardozzi et al., 2012; Mercado et al., 2009; Sitch et al., 2007), and global chemistry models often apply fixed offline vegetation variables (Lamarque et al., 2013). For example, stomatal conductance, which plays a crucial role in regulating water cycle and altering pollution deposition, responds dynamically to vegetation biophysics and environmental stressors at various spatiotemporal scales (Franks et al., 2017; Hetherington and Woodward, 2003). However, these processes are either missing or

https://doi.org/10.5194/gmd-2019-281
Preprint. Discussion started: 30 October 2019

lack of temporal variations in most current chemical transport models (Verbeke et al., 2015). The fully two-way coupling between biosphere and chemistry is necessary to better quantify the responses of ecosystems and pollution to global changes.

In this study, we develop the GC-YIBs model by implementing the Yale Interactive terrestrial Biosphere (YIBs) model version 1.0 (Yue and Unger, 2015) into the chemical transport model (CTM) GEOS-Chem version 12.0.0 (http://wiki.seas.harvard.edu/ geos-chem/index.php/GEOS-Chem_12#12.0.0). The GEOS-Chem (short as GC thereafter) model has been widely used in episode prediction (Cui et al., 2016), source attribution (D'Andrea et al., 2016; Dunker et al., 2017; Lu et al., 2019; Ni et al., 2018), future pollution projection (Ramnarine et al., 2019; Yue et al., 2015), health risk assessment (Xie et al., 2019), and so on. The standard GC model uses prescribed vegetation parameters and as a result cannot depict the changes in chemical components due to biosphere-pollution interactions. The updated GC-YIBs model links atmospheric chemistry with biosphere in a two-way coupling such that changes in chemical components or vegetation will simultaneously feed back to influence the other systems. Here, we evaluate the dynamically simulated dry deposition and leaf area index (LAI) from GC-YIBs and examine the consequent impacts on surface O_3. We also quantify the detrimental effects of O_3 on gross primary productivity (GPP) using instant pollution concentrations from the chemical module. The next section describes the GC-YIBs model and the evaluation data. Section 3 compares simulated O_3 from GC-YIBs with

https://doi.org/10.5194/gmd-2019-281
Preprint. Discussion started: 30 October 2019

that from the original GC models and explores the causes of differences. Section 4 quantifies O_3 damaging effects to global GPP using the GC-YIBs model. The last section summarizes progresses and discusses the next-step tasks to optimize the GC-YIBs model.

2 Methods and data

2.1 Descriptions of the YIBs model

YIBs is a terrestrial vegetation model designed to simulate land carbon cycle with dynamical prediction of LAI and tree height (Yue and Unger, 2015). The model considers 9 plant functional types (PFTs), including evergreen needleleaf forest, deciduous broadleaf forest, evergreen broadleaf forest, shrubland, tundra, C_3/C_4 grass, and C_3/C_4 crops. The satellite-based land types and cover fraction are aggregated into these 9 PFTs and used as input. The YIBs is driven with hourly 2-D meteorology and 3-D soil variables (6 layers) from the Modern-Era Retrospective analysis for Research and Applications, version 2 (MERRA2).

The YIBs uses the model of Ball and Berry (Baldocchi et al., 1987) to compute leaf stomatal conductance:

$$g_s = \frac{1}{r_s} = m \frac{A_{net}}{c_s} RH + b \tag{1}$$

where r_s is the leaf stomatal resistance; m is the empirical slope of the Ball-Berry stomatal conductance equation and is affected by water stress; c_s is the CO_2 concentration at the leaf surface; RH is the relative humidity of atmosphere; b

https://doi.org/10.5194/gmd-2019-281
Preprint. Discussion started: 30 October 2019

Geoscientific Model Development
Discussions

represents the minimum leaf stomatal conductance when net carbon assimilation (A_{net}) is 0. For different PFTs, appropriate photosynthetic parameters are derived from the Community Land Model (CLM) (Bonan et al., 2011).

The net carbon assimilation for C_3 and C_4 plants is computed based on well-established Michaelis–Menten enzyme-kinetics scheme (Farquhar et al., 1980; Voncaemmerer and Farquhar, 1981):

$$A_{net} = \min(J_c, J_e, J_s) - R_d \quad (2)$$

Where J_c, J_e and J_s represent the Rubiso-limited photosynthesis, the RuBP-limited photosynthesis, and the product-limited photosynthesis, respectively. They are all parameterized as functions of the maximum carboxylation capacity (Collatz et al., 1991) and meteorological variables (e.g., temperature, radiation, and CO_2 concentrations).

In addition, the YIBs model implements the scheme for O_3 damage on vegetation proposed by Sitch et al. (2007). The scheme directly modifies photosynthesis using a semi-mechanistic parameterization, which in turn affects stomatal conductance. The O_3 damage factor is considered as the function of stomatal O_3 flux:

$$F = \begin{cases} -a\left(F_{O_3} - T_{O_3}\right), & F_{O_3} > T_{O_3} \\ 0, & F_{O_3} \le T_{O_3} \end{cases} \quad (3)$$

Where a represents the damaging sensitivity and T_{O_3} represents the O_3 flux threshold. For a specific PFT, the coefficient a varies from low to high to represent a range of uncertainties. T_{O_3} is a critical threshold for O_3 damage and varies with PFTs.

https://doi.org/10.5194/gmd-2019-281
Preprint. Discussion started: 30 October 2019

The F becomes negative only if F_{O_3} is higher than T_{O_3}. Stomatal O_3 flux F_{O_3} is dependent on both stomatal resistance and ambient $[O_3]$:

$$F_{O_3} = \frac{[O_3]}{r_b + k \cdot r_s} \quad (4)$$

where $[O_3]$ represents O_3 concentration at top of the canopy, r_b represents the boundary layer resistance, and r_s represents the stomatal resistance. The Sitch et al. (2007) scheme within the YIBs framework has been well evaluated against hundreds of observations globally (Yue and Unger, 2018) and regionally (Yuan et al., 2017; Yue et al., 2016).

2.2 Descriptions of the GEOS-Chem model

GC is a global 3-D model of atmospheric compositions with fully coupled O_3-NO_x-hydrocarbon-aerosol chemical mechanisms (Gantt et al., 2015; Lee et al., 2017; Ni et al., 2018). In this study, we use GC version 12.0.0 driven by assimilated meteorology from MERRA2 with a horizontal resolution of 4° latitude by 5° longitude and 47 vertical layers from surface to 0.01 hPa.

In GC, terrestrial vegetation modulates tropospheric O_3 mainly through LAI and canopy stomatal conductance, which affect both the sources and sinks of tropospheric O_3 through changes in BVOC emissions, soil NO_x emissions, and dry deposition (Zhou et al., 2018). BVOC emissions are calculated based on a baseline emission factor parameterized as the function of light, temperature, leaf age, soil moisture, LAI, and CO_2 inhibition within the Model of Emissions of Gasses and Aerosols from

https://doi.org/10.5194/gmd-2019-281
Preprint. Discussion started: 30 October 2019

Nature (MEGAN v2.1) (Guenther et al., 2006). Soil NO_x emission is computed based on the scheme of Hudman et al. (2012) and further modulated by a reduction factor to account for within-canopy NO_x deposition (Rogers and Whitman, 1991). The dry deposition velocity (V_d) for O_3 is computed based on a resistance-in-series model within GC:

$$V_d = \frac{1}{R_a + R_b + R_c} \tag{5}$$

where R_a is the aerodynamic resistance representing the ability of the airflow to bring gases or particles close to the surface and is dependent mainly on the atmospheric turbulence structure and the height considered. R_b is the boundary resistance driven by the characteristics of surface (surface roughness) and gas/particle (molecular diffusivity). R_a and R_b are calculated from the global climate models (GCM) meteorological variables (Jacob et al., 1992). The surface resistance R_c is determined by the affinity of surface for the chemical compound. For O_3 over vegetated regions, V_d is mainly driven by R_c during daytime because the effects of R_a and R_b are generally small. Surface resistances R_c are computed using the Wesely (1989) canopy model with some improvements, including explicit dependence of canopy stomatal resistances on LAI (Gao and Wesely, 1995) and direct/diffuse PAR within the canopy (Baldocchi et al., 1987):

$$\frac{1}{R_c} = \frac{1}{R_s + R_m} + \frac{1}{R_{lu}} + \frac{1}{R_{cl}} + \frac{1}{R_g} \tag{6}$$

where R_s is the stomatal resistance, R_m is the leaf mesophyll resistance (R_m = 0 s cm^{-1} for O_3), R_{lu} is the upper canopy or leaf cuticle resistance, R_{cl} is the lower

https://doi.org/10.5194/gmd-2019-281
Preprint. Discussion started: 30 October 2019

canopy resistance. R_s is calculated based on minimum stomatal resistance (r_s), solar radiation (G), surface air temperature (T_s), and the molecular diffusivities (D_{H_2O} and D_x) for a specific gas x:

$$R_s = r_s\left\{1+\frac{1}{[200(G+0.1)]^2}\right\}\left\{\frac{400}{T_s(40-T_s)}\right\}\frac{D_{H_2O}}{D_x} \quad (7)$$

In GC, the above parameters related to R_c have prescribed values for 11 deposition land types, including snow/ice, deciduous forest, coniferous forest, agricultural land, shrub/grassland, amazon forest, tundra, desert, wetland, urban and water (Jacob et al., 1992; Wesely, 1989).

The Olson 2001 land cover map used in GC version 12.0.0 has a native resolution of 0.25°×0.25° and 74 land types (Olson et al., 2001). Each of the Olson land types is associated with a corresponding deposition land type with prescribed parameters. There are 74 Olson land types but only 11 deposition land types, suggesting that many of the Olson land types share the same deposition parameters. At specific grids (4°×5° or 2°×2.5°), dry deposition velocity is calculated as the weighted sum of native resolution (0.25°×0.25°).

2.3 Implementation of YIBs into GEOS-Chem (GC-YIBs)

In this study, GC model time steps are set to 30 min for transport and convection and 60 min for emissions and chemistry. In the online GC-YIBs configuration, GC provides the hourly meteorology and surface [O_3] to YIBs. Without YIBs implementation, the GC model computes O_3 dry deposition velocity using prescribed

https://doi.org/10.5194/gmd-2019-281
Preprint. Discussion started: 30 October 2019

LAI and parameterized canopy stomatal resistance (R_s), and as a result ignore feedbacks from ecosystems (details in 2.2). With YIBs embedded, daily LAI and hourly stomatal conductance are dynamically predicted for the dry deposition scheme within the GC model. The online-simulated surface [O_3] affects carbon assimilation and canopy stomatal conductance, in turn, the online-simulated vegetation variables such as LAI and stomatal conductance affect both the sources and sinks of O_3 by altering precursor emissions and dry deposition at the 1-hour integration time step. The above processes are summarized in Fig. 1. To preserve the corresponding relationship between vegetation parameters and land cover map in the GC-YIBs model, we replace the Olson 2001 land cover map in GC with satellite-retrieved land cover dataset used by YIBs (Defries et al., 2000; Hanninen and Kramer, 2007). Stomatal resistance is first calculated for each of 9 PFTs at individual grid cells. The dry deposition velocity is then computed based on the area-weighted sum of stomatal resistance over all PFTs within the same grid.

2.4 Model simulations

We conduct six simulations to evaluate the performance of GC-YIBs and to quantify global O_3 damage to vegetation (Table 1): (i) Offline, a control run using the offline GC-YIBs model. The YIBs module shares the same meteorological forcing as the GC module and predicts both GPP and LAI. However, predicted vegetation variables are not fed into GC, which is instead driven by prescribed LAI from Moderate Resolution Imaging Spectroradiometer (MODIS) product and parameterized canopy stomatal

https://doi.org/10.5194/gmd-2019-281
Preprint. Discussion started: 30 October 2019

conductance proposed by Gao and Wesely (1995). (ii) Online_LAI, a sensitive run using online GC-YIBs with dynamically predicted daily LAI from YIBs but original parameterizations of stomatal conductance. (iii) Online_GS, another sensitive run using YIBs predicted stomatal conductance but prescribed MODIS LAI. (iv) Online_ALL, in which both YIBs predicted LAI and stomatal conductance are used for GC. (v) Online_ALL_HS, the same as Online_ALL except that predicted surface O_3 damages plant photosynthesis with high sensitivities. (vi) Online_ALL_LS, the same as Online_ALL_HS but with low O_3 damaging sensitivities. Each simulation is run from 2006 to 2012 with the first 4 years for spin-up, and results from 2010 to 2012 are used to evaluate the online GC-YIBs model. The differences between Online_ALL and Online_GS (Online_LAI) represent the effects of coupled LAI (stomatal conductance) on simulated [O_3]. Differences between Offline and Online_ALL then represent joint effects of coupled LAI and stomatal conductance. The last three runs are used to quantify the global O_3 damage on ecosystem productivity.

2.5 Validation data

We use observed LAI data for 2010–2012 from the MODIS product. Benchmark GPP product of 2010–2012 is estimated by upscaling ground-based FLUXNET eddy covariance data using a model tree ensemble approach (Jung et al., 2009). Measurements of surface [O_3] over North America and Europe are provided by the Global Gridded Surface Ozone Dataset (Sofen et al., 2016), and those over China are

https://doi.org/10.5194/gmd-2019-281
Preprint. Discussion started: 30 October 2019

Geoscientific Model Development
Discussions

interpolated from data at ~1500 sites operated by China's Ministry of Ecology and Environment (http://english.mee.gov.cn). We perform literature research to collect data of dry deposition velocity from 3 deciduous forest, 2 amazon forest, and 4 coniferous forest sites (Table 2).

3 Results

3.1 Evaluation of offline GC-YIBs model

The simulated GPP and LAI are compared with observations for the period of 2010-2012 (Fig. 2). Observed LAI and benchmark GPP both show high values in the tropics and medium values in the northern mid-high latitudes. Compared to observations, the GC-YIBs model forced with MERRA2 meteorology depicts similar spatial distributions, with spatial correlation coefficients of 0.83 (p <0.01) for GPP and 0.86 (p <0.01) for LAI. Although the model overestimates LAI in the tropics and northern high latitudes by 1-2 m^2 m^{-2}, the simulated global area-weighted LAI (1.42 m^2 m^{-2}) is close to observations (1.33 m^2 m^{-2}) with a normalized mean bias (NMB) of 6.7%. Similar to LAI, the global NMB for GPP is only 7.1%, though there are substantial regional biases especially in Amazon and central Africa. Such differences are in part attributed to the underestimation of GPP for tropical rainforest in the benchmark product, because the recent simulations at eight rainforest sites with the YIBs model driven by a different meteorology dataset (Yue and Unger, 2015) reproduced ground-based observations well (Yue and Unger, 2018)

https://doi.org/10.5194/gmd-2019-281
Preprint. Discussion started: 30 October 2019

We then evaluate simulated annual mean surface [O_3] during 2010-2012 (Fig. 3). The simulated high values are mainly located in the mid-latitudes of Northern Hemisphere (NH, Fig. 3a). Compared to observations, simulations show reasonable spatial distribution with a correlation coefficient of 0.63 (p <0.01). Although offline GC-YIBs model overestimates annual [O_3] in southern China while predicts lower values in western Europe and western U.S., the simulated area-weighted surface [O_3] (45.4 ppbv) is only 6% higher than observations (42.8 ppbv). Predicted summertime surface [O_3] instead shows positive biases in eastern U.S. and Europe (Fig. S1), consistent with previous evaluations using the GC model (Schiferl and Heald, 2018; Travis et al., 2016; Yue and Unger, 2018).

3.2 Changes of surface O_3 in online GC-YIBs model

Surface O_3 is changed by the coupling of LAI and stomatal conductance (Fig. 4). Global [O_3] shows similar patterns between offline (Fig. 3a) and online (Fig. 4a) simulations. However, the online GC-YIBs predicts larger [O_3] of 0.5-2 ppbv in the mid-high latitudes of NH, leading to an average enhancement of [O_3] by 0.22 ppbv compared to offline simulations (Fig. 4b). Regionally, some negative changes of 1-2 ppbv can be found at the tropical regions. With sensitivity experiments Online_LAI and Online_GS (Table. 1), we separate the contributions of LAI and stomatal conductance changes to Δ[O_3]. It is found that Δ[O_3] between Online_ALL and Online_LAI (Fig. 4c) resembles the total Δ[O_3] pattern (Fig. 4b), suggesting that changes in stomatal conductance play the dominant role in regulating surface [O_3]. As

https://doi.org/10.5194/gmd-2019-281
Preprint. Discussion started: 30 October 2019

Geoscientific Model Development
Discussions

a comparison, $\Delta[O_3]$ values between Online_ALL and Online_GS show limited changes globally (by 0.05 ppbv) and moderate changes in tropical regions (Fig. 4d), mainly because the LAI predicted by YIBs is close to MODIS LAI used in GC (Fig. 2). It is noticed that the average $\Delta[O_3]$ in Fig. 4b is not equal to the sum of Fig. 4c and Fig. 4d, because of the non-linear effects.

We further explore the possible causes of differences in simulated $[O_3]$ between online and offline GC-YIBs models. Fig. 5 shows simulated annual O_3 dry deposition velocity from online GC-YIBs model and its changes in different sensitivity experiments. The global average velocity is 0.25 cm s^{-1} with regional maximum of 0.5-0.7 cm s^{-1} in tropical rainforest (Fig. 5a), especially over Amazon and central Africa where high ecosystem productivity is observed (Fig. 2). With implementation of YIBs into GC, simulated dry deposition velocity increases over tropical regions but decreases in mid-high latitudes of NH (Fig. 5b). Larger dry deposition results in lower $[O_3]$ in the tropics, while smaller dry deposition increases $[O_3]$ in boreal regions. Such spatial patterns are broadly consistent with $\Delta[O_3]$ in online GC-YIBs (Fig. 4b), suggesting that changes of dry deposition velocity are the dominant drivers of O_3 changes. Both the updated LAI and stomatal conductance influence dry deposition. Sensitivity experiments further show that changes in dry deposition are mainly driven by coupled canopy stomatal conductance (Fig. 5c) instead of LAI (Fig. 5d), though the latter contributes to the enhanced dry deposition in the tropics.

The original GC dry deposition scheme applies fixed parameters for stomatal conductance of a specific land type (Fig. 6). The updated GC-YIBs model instead calculates stomatal conductance as a function of photosynthesis and environmental forcings (Equation 1). As a result, predicted dry deposition exhibits discrepancies among biomes (Fig. 7). For agricultural land and shrub/grassland, the simulated O_3 dry deposition velocity for online GC-YIBs model is close to GC model with NMBs of 3%, -2% and correlation coefficients of 0.96, 0.97, respectively. However, the simulated dry deposition velocity in online GC-YIBs is lower than GC by 18% for deciduous forest and 14% coniferous forest, but larger by 17% for Amazon forest. Such changes match the spatial pattern of dry deposition shown in Fig. 5b.

Since the changes of O_3 dry deposition velocity are mainly found in deciduous forest, coniferous forest, and amazon forest, we collect data at 9 sites across these three biomes to evaluate the online GC-YIBs model (Table. 2 and Fig. 6). For the 5 samples at deciduous forest, the normalized mean error (NME) decreases from 50% in GC model to 27% in GC-YIBs with lower relative errors in all sites (Fig. 8). Predictions with the GC-YIBs also show large improvements over coniferous forest, where 6 out of 9 samples showing lower (decreases from 48% in GC to 35% in GC-YIBs) errors. For amazon forest, the GC-YIBs model significantly improves the prediction at one site (117.9°E, 4.9°N) where the original error of -0.17 cm s^{-1} is limited to only 0.03 cm s^{-1}. However, the new model does not improve the prediction at the other amazon forest site. Overall, the simulated daytime O_3 dry deposition velocities in online

https://doi.org/10.5194/gmd-2019-281
Preprint. Discussion started: 30 October 2019

Geoscientific Model Development Discussions
Open Access

GC-YIBs model are closer to observations than those in GC model with smaller NME (27% vs. 35%), root-mean-square errors (RMSE, 0.19 vs. 0.24) and higher correlation coefficients (0.85 vs. 0.76). Such improvements consolidate our strategies in updating GC model to the fully coupled GC-YIBs model.

3.3 Assessment of global O_3 damages to vegetation

An important feature of GC-YIBs is the inclusion of online vegetation damages by surface O_3. Here, we quantify the global O_3 damages to GPP and LAI by conducting Online_ALL_HS and Online_ALL_LS simulations (Fig. 9). Due to O_3 damaging, annual GPP declines from -2% (low sensitivity) to -5% (high sensitivity) on the global scale. Regionally, O_3 decreases GPP as high as 11% in the eastern U.S. and up to 15% in eastern China at the high sensitivity (Figs. 9a, b). Such strong damages are related to (i) high ambient [O_3] due to anthropogenic emissions and (ii) large stomatal conductance due to active ecosystem productivity in monsoon areas. The O_3 effects are moderate in tropical areas, where stomatal conductance is also high while [O_3] is very low (Fig. 4a) due to limited anthropogenic emissions. Furthermore, O_3-induced GPP reductions are also small in western U.S. and western Asia. Although [O_3] is high over these semi-arid regions (Fig. 4a), the drought stress decreases stomatal conductance and consequently constrains the O_3 uptake. The damages to LAI (Figs. 9c, d) generally follow the pattern of GPP reductions (Figs. 9a, b) but with lower magnitude. These results are slightly different from our previous studies which used prescribed LAI and/or surface [O_3] in the simulations (Yue and Unger, 2014, 2015).

https://doi.org/10.5194/gmd-2019-281
Preprint. Discussion started: 30 October 2019

Geoscientific Model Development Discussions

4 Conclusions and discussion

The terrestrial biosphere and atmospheric chemistry interact through a series of feedbacks (Green et al., 2017). Among biosphere-chemistry interactions, dry deposition plays a key role in the exchange of compounds and acts as an important sink for several air pollutants (Verbeke et al., 2015). However, dry deposition is simply parameterized in most of current CTMs (Hardacre et al., 2015). For all chemical species considered in GC model, stomatal resistance R_c is simply calculated as the function of minimum stomatal resistance and meteorological forcings. Such parameterization not only induces biases, but also ignores the feedbacks from biosphere-chemistry interactions. For example, recent studies revealed that O_3-induced damages to vegetation could reduce stomatal conductance and in turn alter ambient O_3 level (Sadiq et al., 2017; Zhou et al., 2018). In this study, we implement YIBs into the GC model with fully interactive surface O_3 and terrestrial biosphere. The dynamically predicted LAI and stomatal conductance from YIBs are instantly provided to GC, meanwhile the prognostic O_3 simulated by GC is simultaneously affecting vegetation biophysics in YIBs. With these updates, simulated daytime O_3 dry deposition velocities in GC-YIBs are closer to observations than those in original GC model.

An earlier study updated dry deposition scheme in the Community Earth System Model (CESM) by implementing the leaf and stomatal resistances (Val Martin et al., 2014). Compared to that work, the magnitudes of $\Delta[O_3]$ in our simulations are smaller

https://doi.org/10.5194/gmd-2019-281
Preprint. Discussion started: 30 October 2019

in northern America, eastern Europe, and southern China. This might be because the original dry deposition scheme in the GC model (see validation in Fig. 7) is better than that in CESM, leaving limited potentials for improvements. In GC, the leaf cuticular resistance (R_{lu}) is dependent on LAI (Gao and Wesely, 1995), while the original calculation of R_{lu} in CESM does not include LAI (Wesely, 1989). In addition, differences in the canopy schemes for stomatal conductance between YIBs and Community Land Model (CLM) may cause different responses in dry deposition, which is changed by -0.12 to 0.16 cm s^{-1} in GC-YIBs but much larger by -0.15 to 0.25 cm s^{-1} in CESM (Val Martin et al., 2014). Moreover, the GC-YIBs is driven with prescribed reanalysis while CESM dynamically predicts climatic variables. Perturbations of meteorology in response to terrestrial properties may further magnify the variations in atmospheric components in CESM.

Although we implement YIBs into GC with fully interactive surface O_3 and terrestrial biosphere, it should be noted that considerable limits still exist and further developments are required for GC-YIBs. (1) Atmospheric nitrogen alters plant growth and further influences both the sources and sinks of surface O_3 through surface–atmosphere exchange processes (Zhao et al., 2017). However, the YIBs model currently utilizes a fixed nitrogen level and does not include an interactive nitrogen cycle, which may induce uncertainties in simulating carbon fluxes. (2) The current GC-YIBs is limited to a low resolution due to slow computational speed and high computational costs for long-term integrations. The GC model, even at the 2°×2.5°

resolution, takes days to simulate 1 model year due to comprehensive parameterizations of physical and chemical processes. Such low speed constrains long-term spin up required by dynamical vegetation models. (3) Validity of $\Delta[O_3]$, especially those at high latitudes in NH, cannot be directly evaluated due to a lack of measurements. Although changes of dry deposition show improvements in GC-YIBs, the ultimate effects on surface $[O_3]$ remain unclear within the original GC framework.

Despite these deficits, the development of GC-YIBs provides a unique tool for studying biosphere-chemistry interactions. In the future, we will extend our applications in: (1) Air pollution impacts on biosphere, including both O_3 and aerosol effects. The GC-YIBs model can predict atmospheric aerosols, which affect both direct and diffuse radiation through the Rapid Radiative Transfer Model for GCMs (RRTMG) in the GC module (Schiferl and Heald, 2018). The diffuse fertilization effects in the YIBs model have been fully evaluated (Yue and Unger, 2018), and as a result we can quantify the impacts of aerosols on terrestrial ecosystems. (2) Multiple schemes for BVOC emissions. The YIBs model incorporates both MEGAN (Guenther et al., 2006) and photosynthesis-dependent (Unger, 2013) isoprene emission schemes (Yue and Unger, 2015). The two schemes within the GC-YIBs framework can be used and compared for simulations of BVOC and consequent air pollution (e.g., O_3, secondary organic aerosols). (3) Biosphere-chemistry feedbacks to air pollution. The effects of air pollution on the biosphere include changes in stomatal conductance, LAI, and BVOC emissions, which in turn modify the sources and sinks of atmospheric components. Only a few studies have quantified these feedbacks for O_3-vegetation interactions (Sadiq et al., 2017; Zhou et al., 2018). We can explore the full biosphere-chemistry coupling for both O_3 and aerosols using the GC-YIBs model in the future.

Code availability

The YIBs model was developed by Xu Yue and Nadine Unger with code sharing at https://github.com/YIBS01/YIBS_site. The GEOS-Chem model was developed by the Atmospheric Chemistry Modeling Group at Harvard University led by Prof. Daniel Jacob and is publicly available at http://acmg.seas.harvard.edu/geos/. The source codes for the GC-YIBs model is archived at https://github.com/leiyd001/GC-YIBs.

Author contributions. Xu Yue conceived the study. Yadong Lei and Xu Yue were responsible for model coupling, simulations, results analysis and paper writing. All co-authors improved and prepared the manuscript.

Competing interests. The authors declare that they have no conflict of interest.

Acknowledgements. This work is supported by the National Key Research and Development Program of China (grant no. SQ2019YFA060013-02) and National Natural Science Foundation of China (grant no. 41975155).

References

Baldocchi, D. D., Hicks, B. B., and Camara, P.: A Canopy Stomatal-Resistance Model for Gaseous Deposition to Vegetated Surfaces, Atmospheric Environment, 21, 91-101, 1987.

Bonan, G. B., Lawrence, P. J., Oleson, K. W., Levis, S., Jung, M., Reichstein, M., Lawrence, D. M., and Swenson, S. C.: Improving canopy processes in the Community Land Model version 4 (CLM4) using global flux fields empirically inferred from FLUXNET data, J Geophys Res-Biogeo, 116, 2011.

Carslaw, K. S., Boucher, O., Spracklen, D. V., Mann, G. W., Rae, J. G. L., Woodward, S., and Kulmala, M.: A review of natural aerosol interactions and feedbacks within the Earth system, Atmospheric Chemistry and Physics, 10, 1701-1737, 2010.

Coe, H., Gallagher, M. W., Choularton, T. W., and Dore, C.: Canopy scale measurements of stomatal and cuticular O3 uptake by Sitka spruce, Atmospheric Environment, 29, 1413-1423, 1995.

Collatz, G. J., Ball, J. T., Grivet, C., and Berry, J. A.: Physiological and Environmental-Regulation of Stomatal Conductance, Photosynthesis and Transpiration - a Model That Includes a Laminar Boundary-Layer, Agr Forest Meteorol, 54, 107-136, 1991.

Cui, Y. Z., Lin, J. T., Song, C. Q., Liu, M. Y., Yan, Y. Y., Xu, Y., and Huang, B.: Rapid growth in nitrogen dioxide pollution over Western China, 2005-2013, Atmospheric Chemistry and Physics, 16, 6207-6221, 2016.

D'Andrea, S. D., Ng, J. Y., Kodros, J. K., Atwood, S. A., Wheeler, M. J., Macdonald, A. M., Leaitch, W. R., and Pierce, J. R.: Source attribution of aerosol size distributions and model evaluation using Whistler Mountain measurements and GEOS-Chem-TOMAS simulations, Atmospheric Chemistry and Physics, 16, 383-396, 2016.

Defries, R. S., Hansen, M. C., Townshend, J. R. G., Janetos, A. C., and Loveland, T. R.: A new global 1-km dataset of percentage tree cover derived from remote sensing, Glob Change Biol, 6, 247-254, 2000.

Dunker, A. M., Koo, B., and Yarwood, G.: Contributions of foreign, domestic and natural emissions to US ozone estimated using the path-integral method in CAMx nested within GEOS-Chem, Atmospheric Chemistry and Physics, 17, 12553-12571, 2017.

Farquhar, G. D., Caemmerer, S. V., and Berry, J. A.: A Biochemical-Model of Photosynthetic Co2 Assimilation in Leaves of C-3 Species, Planta, 149, 78-90, 1980.

Fowler, D., Nemitz, E., Misztal, P., Di Marco, C., Skiba, U., Ryder, J., Helfter, C., Cape, J. N., Owen, S., Dorsey, J., Gallagher, M. W., Coyle, M., Phillips, G., Davison, B., Langford, B., MacKenzie, R., Muller, J., Siong, J., Dari-Salisburgo, C., Di Carlo, P., Aruffo, E., Giammaria, F., Pyle, J. A., and Hewitt, C. N.: Effects of land use on surface-atmosphere exchanges of trace gases and energy in Borneo: comparing fluxes over oil palm plantations and a rainforest, Philos T R Soc B, 366, 3196-3209, 2011.

https://doi.org/10.5194/gmd-2019-281
Preprint. Discussion started: 30 October 2019

Geoscientific Model Development
Discussions

Fowler, D., Pilegaard, K., Sutton, M. A., Ambus, P., Raivonen, M., Duyzer, J., Simpson, D., Fagerli, H., Fuzzi, S., Schjoerring, J. K., Granier, C., Neftel, A., Isaksen, I. S. A., Laj, P., Maione, M., Monks, P. S., Burkhardt, J., Daemmgen, U., Neirynck, J., Personne, E., Wichink-Kruit, R., Butterbach-Bahl, K., Flechard, C., Tuovinen, J. P., Coyle, M., Gerosa, G., Loubet, B., Altimir, N., Gruenhage, L., Ammann, C., Cieslik, S., Paoletti, E., Mikkelsen, T. N., Ro-Poulsen, H., Cellier, P., Cape, J. N., Horvath, L., Loreto, F., Niinemets, U., Palmer, P. I., Rinne, J., Misztal, P., Nemitz, E., Nilsson, D., Pryor, S., Gallagher, M. W., Vesala, T., Skiba, U., Brueggemann, N., Zechmeister-Boltenstern, S., Williams, J., O'Dowd, C., Facchini, M. C., de Leeuw, G., Flossman, A., Chaumerliac, N., and Erisman, J. W.: Atmospheric composition change: Ecosystems-Atmosphere interactions, Atmospheric Environment, 43, 5193-5267, 2009.

Franks, P. J., Berry, J. A., Lombardozzi, D. L., and Bonan, G. B.: Stomatal Function across Temporal and Spatial Scales: Deep-Time Trends, Land-Atmosphere Coupling and Global Models, Plant Physiol, 174, 583-602, 2017.

Gantt, B., Johnson, M. S., Crippa, M., Prevot, A. S. H., and Meskhidze, N.: Implementing marine organic aerosols into the GEOS-Chem model, Geoscientific Model Development, 8, 619-629, 2015.

Gao and Wesely: Modeling gaseous dry deposition over regional scales with satellite observation, Atmosphere Environment, 1995. 1995.

Green, J. K., Konings, A. G., Alemohammad, S. H., Berry, J., Entekhabi, D., Kolassa, J., Lee, J. E., and Gentine, P.: Regionally strong feedbacks between the atmosphere and terrestrial biosphere, Nat Geosci, 10, 410-+, 2017.

Guenther, A., Karl, T., Harley, P., Wiedinmyer, C., Palmer, P. I., and Geron, C.: Estimates of global terrestrial isoprene emissions using MEGAN (Model of Emissions of Gases and Aerosols from Nature), Atmospheric Chemistry and Physics, 6, 3181-3210, 2006.

Hanninen, H. and Kramer, K.: A framework for modelling the annual cycle of trees in boreal and temperate regions, Silva Fenn, 41, 167-205, 2007.

Hardacre, C., Wild, O., and Emberson, L.: An evaluation of ozone dry deposition in global scale chemistry climate models, Atmospheric Chemistry and Physics, 15, 6419-6436, 2015.

Hetherington, A. M. and Woodward, F. I.: The role of stomata in sensing and driving environmental change, Nature, 424, 901-908, 2003.

Hole, L. R., Semb, A., and Torseth, K.: Ozone deposition to a temperate coniferous forest in Norway; gradient method measurements and comparison with the EMEP deposition module, Atmospheric Environment, 38, 2217-2223, 2004.

Hungate, B. A. and Koch, G. W.: Global Environmental Change: Biospheric Impacts and Feedbacks, Encyclopedia of Atmospheric Sciences, 2015. 132-140, 2015.

Jacob, D. J., Wofsy, S. C., Bakwin, P. S., Fan, S. M., Harriss, R. C., Talbot, R. W., Bradshaw, J. D., Sandholm, S. T., Singh, H. B., Browell, E. V., Gregory, G. L., Sachse, G. W., Shipham, M. C., Blake, D. R., and Fitzjarrald, D. R.: Summertime Photochemistry of the Troposphere at High Northern Latitudes, J Geophys Res-Atmos, 97, 16421-16431, 1992.

Jung, M., Reichstein, M., and Bondeau, A.: Towards global empirical upscaling of FLUXNET eddy covariance observations: validation of a model tree ensemble approach using a biosphere model, Biogeosciences, 6, 2001-2013, 2009.
Kleinman, L. I.: Low and High Nox Tropospheric Photochemistry, J Geophys Res-Atmos, 99, 16831-16838, 1994.
Lamarque, J. F., Shindell, D. T., Josse, B., Young, P. J., Cionni, I., Eyring, V., Bergmann, D., Cameron-Smith, P., Collins, W. J., Doherty, R., Dalsoren, S., Faluvegi, G., Folberth, G., Ghan, S. J., Horowitz, L. W., Lee, Y. H., MacKenzie, I. A., Nagashima, T., Naik, V., Plummer, D., Righi, M., Rumbold, S. T., Schulz, M., Skeie, R. B., Stevenson, D. S., Strode, S., Sudo, K., Szopa, S., Voulgarakis, A., and Zeng, G.: The Atmospheric Chemistry and Climate Model Intercomparison Project (ACCMIP): overview and description of models, simulations and climate diagnostics, Geosci Model Dev, 6, 179-206, 2013.
Lee, H. M., Park, R. J., Henze, D. K., Lee, S., Shim, C., Shin, H. J., Moon, K. J., and Woo, J. H.: PM2.5 source attribution for Seoul in May from 2009 to 2013 using GEOS-Chem and its adjoint model, Environmental Pollution, 221, 377-384, 2017.
Lelieveld, J. and Dentener, F. J.: What controls tropospheric ozone?, Journal of Geophysical Research: Atmospheres, 105, 3531-3551, 2000.
Li, K., Jacob, D. J., Liao, H., Shen, L., Zhang, Q., and Bates, K. H.: Anthropogenic drivers of 2013-2017 trends in summer surface ozone in China, Proc Natl Acad Sci U S A, 116, 422-427, 2019.
Lombardozzi, D., Levis, S., Bonan, G., and Sparks, J. P.: Predicting photosynthesis and transpiration responses to ozone: decoupling modeled photosynthesis and stomatal conductance, Biogeosciences, 9, 3113-3130, 2012.
Lu, X., Zhang, L., Chen, Y. F., Zhou, M., Zheng, B., Li, K., Liu, Y. M., Lin, J. T., Fu, T. M., and Zhang, Q.: Exploring 2016-2017 surface ozone pollution over China: source contributions and meteorological influences, Atmospheric Chemistry and Physics, 19, 8339-8361, 2019.
Mahowald, N.: Aerosol Indirect Effect on Biogeochemical Cycles and Climate, Science, 334, 794-796, 2011.
McGrath, J. M., Betzelberger, A. M., Wang, S. W., Shook, E., Zhu, X. G., Long, S. P., and Ainsworth, E. A.: An analysis of ozone damage to historical maize and soybean yields in the United States, P Natl Acad Sci USA, 112, 14390-14395, 2015.
Mercado, L. M., Bellouin, N., Sitch, S., Boucher, O., Huntingford, C., Wild, M., and Cox, P. M.: Impact of changes in diffuse radiation on the global land carbon sink, Nature, 458, 1014-U1087, 2009.
Mikkelsen, T. N., Ro-Poulsen, H., Hovmand, M. F., Jensen, N. O., Pilegaard, K., and Egelov, A. H.: Five-year measurements of ozone fluxes to a Danish Norway spruce canopy, Atmospheric Environment, 38, 2361-2371, 2004.
Munger, J. W., Wofsy, S. C., Bakwin, P. S., Fan, S. M., Goulden, M. L., Daube, B. C., Goldstein, A. H., Moore, K. E., and Fitzjarrald, D. R.: Atmospheric deposition of reactive nitrogen oxides and ozone in a temperate deciduous forest and a subarctic

woodland .1. Measurements and mechanisms, J Geophys Res-Atmos, 101, 12639-12657, 1996.

Ni, R. J., Lin, J. T., Yan, Y. Y., and Lin, W. L.: Foreign and domestic contributions to springtime ozone over China, Atmospheric Chemistry and Physics, 18, 11447-11469, 2018.

Oliver, R. J., Mercado, L. M., Sitch, S., Simpson, D., Medlyn, B. E., Lin, Y.-S., and Folberth, G. A.: Large but decreasing effect of ozone on the European carbon sink, Biogeosciences, 15, 4245-4269, 2018.

Olson, D. M., Dinerstein, E., Wikramanayake, E. D., Burgess, N. D., Powell, G. V. N., Underwood, E. C., D'Amico, J. A., Itoua, I., Strand, H. E., Morrison, J. C., Loucks, C. J., Allnutt, T. F., Ricketts, T. H., Kura, Y., Lamoreux, J. F., Wettengel, W. W., Hedao, P., and Kassem, K. R.: Terrestrial ecoregions of the worlds: A new map of life on Earth, Bioscience, 51, 933-938, 2001.

Park, R. J., Hong, S. K., Kwon, H. A., Kim, S., Guenther, A., Woo, J. H., and Loughner, C. P.: An evaluation of ozone dry deposition simulations in East Asia, Atmospheric Chemistry and Physics, 14, 7929-7940, 2014.

Petroff, A.: Mechanistic study of aerosol dry deposition on vegetated canopies, Radioprotection, 40, S443-S450, 2005.

Ramnarine, E., Kodros, J. K., Hodshire, A. L., Lonsdale, C. R., Alvarado, M. J., and Pierce, J. R.: Effects of near-source coagulation of biomass burning aerosols on global predictions of aerosol size distributions and implications for aerosol radiative effects, Atmospheric Chemistry and Physics, 19, 6561-6577, 2019.

Rogers, J. E. and Whitman, W. B.: Microbial production and consumption of greenhouse gases: methane, nitrogen oxides, and halomethanes, Journal of Environmental Quality, 23, 211-212, 1991.

Sadiq, M., Tai, A. P. K., Lombardozzi, D., and Val Martin, M.: Effects of ozone–vegetation coupling on surface ozone air quality via biogeochemical and meteorological feedbacks, Atmospheric Chemistry and Physics, 17, 3055-3066, 2017.

Schiferl, L. D. and Heald, C. L.: Particulate matter air pollution may offset ozone damage to global crop production, Atmospheric Chemistry and Physics, 18, 5953-5966, 2018.

Sitch, S., Cox, P. M., Collins, W. J., and Huntingford, C.: Indirect radiative forcing of climate change through ozone effects on the land-carbon sink, Nature, 448, 791-794, 2007.

Sofen, E. D., Bowdalo, D., Evans, M. J., Apadula, F., Bonasoni, P., Cupeiro, M., Ellul, R., Galbally, I. E., Girgzdiene, R., and Luppo, S.: Gridded global surface ozone metrics for atmospheric chemistry model evaluation, Earth System Science Data,8,1(2016-02-11), 8, 603-647, 2016.

Travis, K. R., Jacob, D. J., Fisher, J. A., Kim, P. S., Marais, E. A., Zhu, L., Yu, K., Miller, C. C., Yantosca, R. M., Sulprizio, M. P., Thompson, A. M., Wennberg, P. O., Crounse, J. D., St Clair, J. M., Cohen, R. C., Laughner, J. L., Dibb, J. E., Hall, S. R., Ullmann, K., Wolfe, G. M., Pollack, I. B., Peischl, J., Neuman, J. A., and Zhou, X.

L.: Why do models overestimate surface ozone in the Southeast United States?, Atmospheric Chemistry and Physics, 16, 13561-13577, 2016.

Unger, N.: Isoprene emission variability through the twentieth century, J Geophys Res-Atmos, 118, 13606-13613, 2013.

Val Martin, M., Heald, C. L., and Arnold, S. R.: Coupling dry deposition to vegetation phenology in the Community Earth System Model: Implications for the simulation of surface O3, Geophysical Research Letters, 41, 2988-2996, 2014.

Van Dingenen, R., Dentener, F. J., Raes, F., Krol, M. C., Emberson, L., and Cofala, J.: The global impact of ozone on agricultural crop yields under current and future air quality legislation, Atmospheric Environment, 43, 604-618, 2009.

Verbeke, T., Lathière, J., Szopa, S., and de Noblet-Ducoudré, N.: Impact of future land-cover changes on HNO3 and O3 surface dry deposition, Atmospheric Chemistry and Physics, 15, 13555-13568, 2015.

Voncaemmerer, S. and Farquhar, G. D.: Some Relationships between the Biochemistry of Photosynthesis and the Gas-Exchange of Leaves, Planta, 153, 376-387, 1981.

Wesely: Parameterization of surface resistances to gaseous drydeposition in regional-scale numerical models, 1989. 1989.

Wilkinson, S., Mills, G., Illidge, R., and Davies, W. J.: How is ozone pollution reducing our food supply?, J Exp Bot, 63, 527-536, 2012.

Xie, Y., Dai, H. C., Zhang, Y. X., Wu, Y. Z., Hanaoka, T., and Masui, T.: Comparison of health and economic impacts of PM2.5 and ozone pollution in China, Environ Int, 130, 2019.

Yuan, X. Y., Feng, Z. Z., Liu, S., Shang, B., Li, P., Xu, Y. S., and Paoletti, E.: Concentration-and flux-based dose-responses of isoprene emission from poplar leaves and plants exposed to an ozone concentration gradient, Plant Cell Environ, 40, 1960-1971, 2017.

Yue, X., Keenan, T. F., Munger, W., and Unger, N.: Limited effect of ozone reductions on the 20-year photosynthesis trend at Harvard forest, Glob Change Biol, 22, 3750-3759, 2016.

Yue, X., Mickley, L. J., Logan, J. A., Hudman, R. C., Martin, M. V., and Yantosca, R. M.: Impact of 2050 climate change on North American wildfire: consequences for ozone air quality, Atmospheric Chemistry and Physics, 15, 10033-10055, 2015.

Yue, X. and Unger, N.: Fire air pollution reduces global terrestrial productivity, Nat Commun, 9, 5413, 2018.

Yue, X. and Unger, N.: Ozone vegetation damage effects on gross primary productivity in the United States, Atmospheric Chemistry and Physics, 14, 9137-9153, 2014.

Yue, X. and Unger, N.: The Yale Interactive terrestrial Biosphere model version 1.0: description, evaluation and implementation into NASA GISS ModelE2, Geoscientific Model Development, 8, 2399-2417, 2015.

Zhao, Y., Zhang, L., Tai, A. P. K., Chen, Y., and Pan, Y.: Responses of surface ozone air quality to anthropogenic nitrogen deposition in the Northern Hemisphere, Atmospheric Chemistry and Physics, 17, 9781-9796, 2017.

https://doi.org/10.5194/gmd-2019-281
Preprint. Discussion started: 30 October 2019

Zhou, S. S., Tai, A. P. K., Sun, S., Sadiq, M., Heald, C. L., and Geddes, J. A.: Coupling between surface ozone and leaf area index in a chemical transport model: strength of feedback and implications for ozone air quality and vegetation health, Atmospheric Chemistry and Physics, 18, 14133-14148, 2018.

Table 1 Summary of simulations using the GC-YIBs model

Name	Scheme	Ozone effects
Offline	Monthly prescribed MODIS LAI	No
	Original dry deposition scheme	
Online_LAI	Daily dynamically predicted LAI	No
	Original dry deposition scheme	
Online_GS	Monthly prescribed MODIS LAI	No
	Hourly predicted stomatal conductance	
Online_ALL	Daily dynamically predicted LAI	No
	Hourly predicted stomatal conductance	
Online_ALL_HS	Daily dynamically predicted LAI	
	Hourly predicted stomatal conductance	High
	Hourly predicted [O_3] by GC model	
Online_ALL_LS	Daily dynamically predicted LAI	
	Hourly predicted stomatal conductance	Low
	Hourly predicted [O_3] by GC model	

https://doi.org/10.5194/gmd-2019-281
Preprint. Discussion started: 30 October 2019

702 **Table.2** List of measurement sites used for dry deposition evaluation

Land type	Longitude	Latitude	Season	Vd (daytime, cm s^{-1})	Citation
Deciduous forest	80.9°W	44.3°N	summer	0.92	(Padro et al., 1991)
			winter	0.28	
	72.2°W	42.7°N	summer	0.61	(Munger et al., 1996)
			winter	0.28	
	75.2°W	43.6°N	summer	0.82	
Amazon forest	61.8°W	10.1°S	wet	1.1	(Rummel et al., 2007)
	117.9°E	4.9°N	wet	1.0	(Fowler et al., 2011)
Coniferous forest	3.4°W	55.3°N	spring	0.58	(Coe et al., 1995)
	66.7°W	54.8°N	summer	0.26	(Munger et al., 1996)
	11.1°E	60.4°N	spring	0.31	(Hole et al., 2004)
			summer	0.48	
			autumn	0.2	
			winter	0.074	
	8.4°E	56.3°N	spring	0.68	(Mikkelsen et al., 2004)
			summer	0.8	
			autumn	0.83	

703

704

https://doi.org/10.5194/gmd-2019-281
Preprint. Discussion started: 30 October 2019

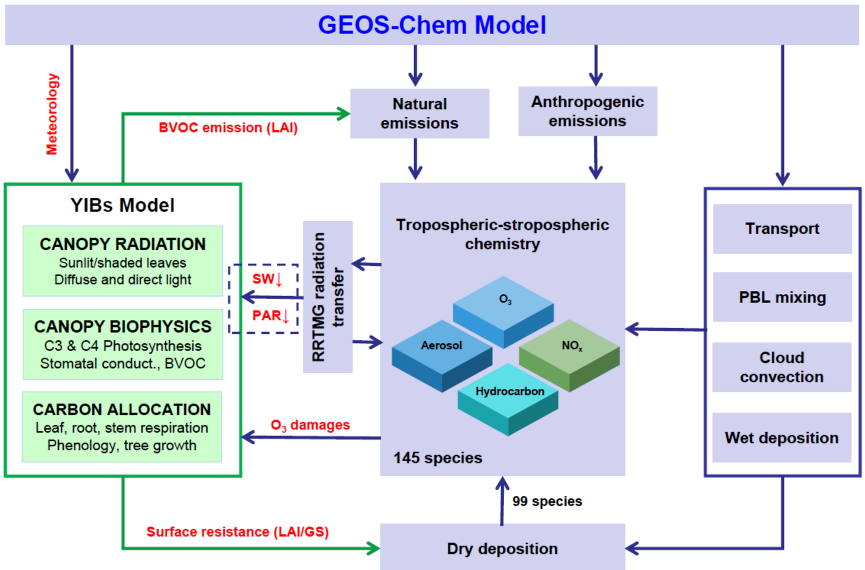

Figure 1 Diagram of the GC-YIBs global carbon-chemistry model. Processes with red fonts are implemented in this study. Processes with blue dashed box will be developed in the future.

https://doi.org/10.5194/gmd-2019-281
Preprint. Discussion started: 30 October 2019

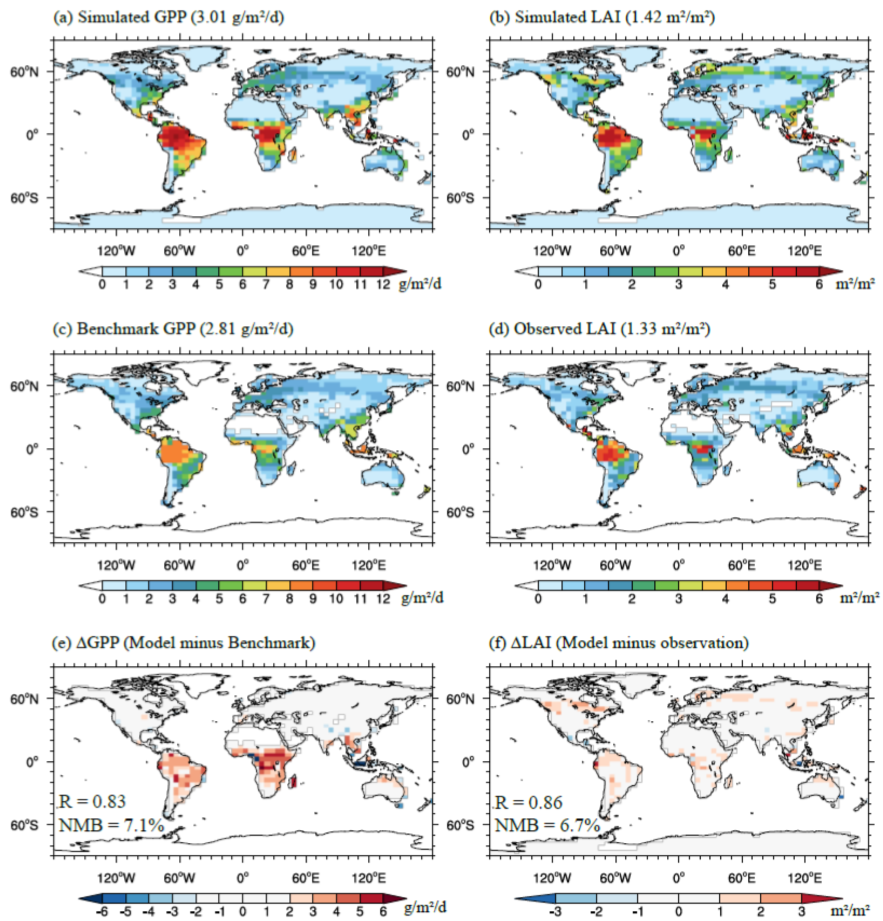

Figure 2 Annual gross primary productivity (GPP) and leaf area index (LAI) from simulations (a, b), observations (c, d), and their differences (e, f) averaged for period of 2010-2012. Global area-weighted GPP and LAI are shown on the title brackets. The correlation coefficients (R) and global normalized mean biases (NMB) are shown in the bottom figures.

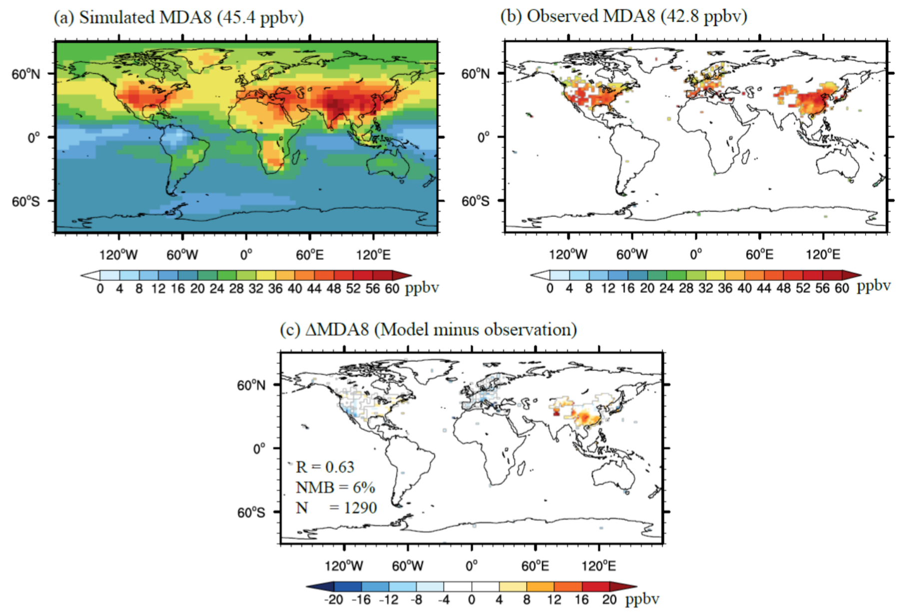

Figure 3 Annual surface O_3 concentrations ($[O_3]$) from simulations (a), observations (b), and their differences (c) averaged for period of 2010-2012. Global area-weighted surface $[O_3]$ over grids with available observations are shown on the title brackets. The correlation coefficient (R) and global normalized mean biases (NMB) are shown in the bottom figures with indication of grid numbers (N) used for statistics.

https://doi.org/10.5194/gmd-2019-281
Preprint. Discussion started: 30 October 2019

Geoscientific Model Development
Discussions
Open Access

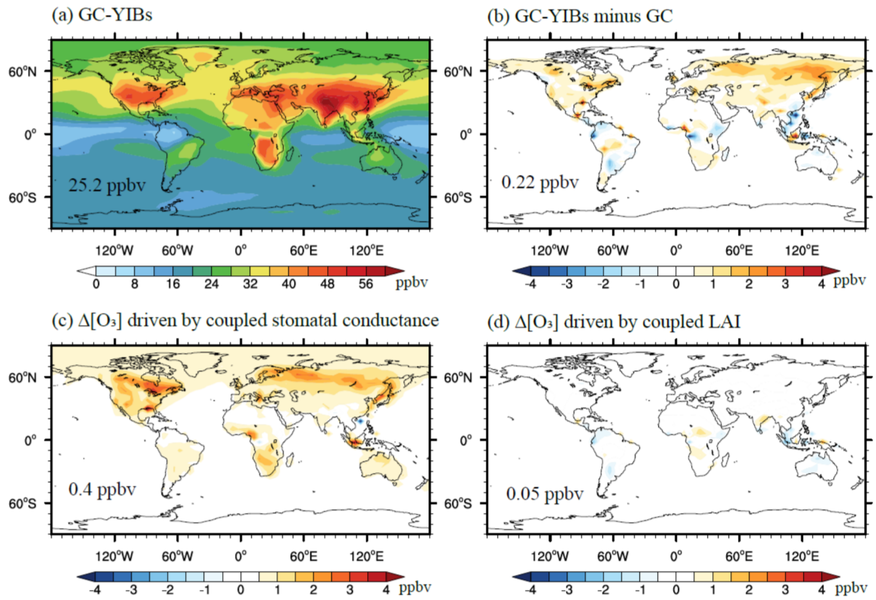

Figure 4 Simulated annual surface [O_3] from online GC-YIBs model (a) and its changes (b-d) relative to offline simulations. Changes of [O_3] are caused by (b) jointly coupled LAI and stomatal conductance (Online_ALL – Offline), (c) coupled stomatal conductance alone (Online_ALL – Online_LAI), and (d) coupled LAI alone (Online_ALL – Online_GS). Global area-weighted [O_3] or Δ[O_3] are shown in the figures.

https://doi.org/10.5194/gmd-2019-281
Preprint. Discussion started: 30 October 2019

Geoscientific Model Development
Discussions

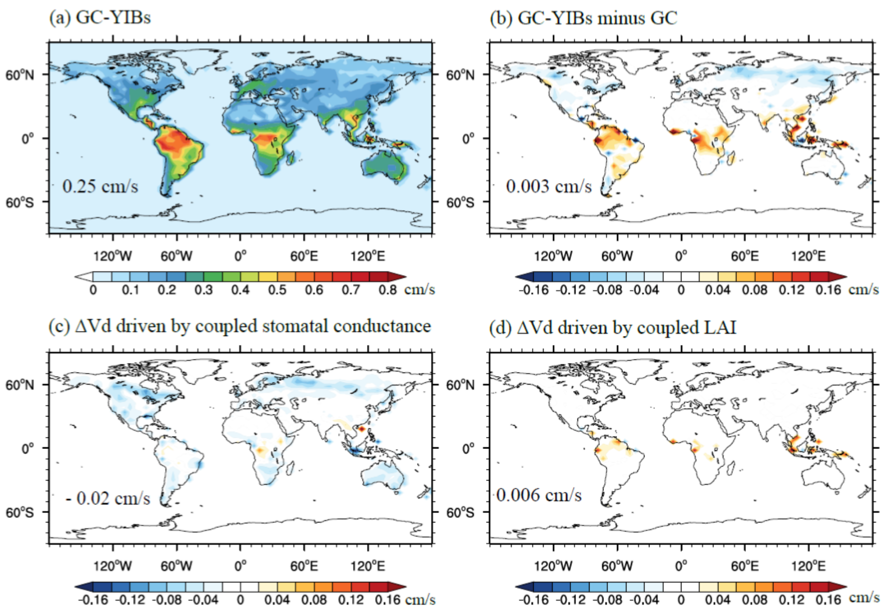

Figure 5 Simulated annual O_3 dry deposition velocity from online GC-YIBs model (a) and its changes caused by coupled LAI and stomatal conductance (b-d) averaged for period of 2010-2012. The changes of dry deposition velocity are driven by (b) coupled LAI and stomatal conductance (Online_ALL – Offline), (c) coupled stomatal conductance alone (Online_ALL – Online_LAI), and (d) coupled LAI alone (Online_ALL – Online_GS). Global area-weighted annual O_3 dry deposition velocity and changes are shown in the figures.

https://doi.org/10.5194/gmd-2019-281
Preprint. Discussion started: 30 October 2019

Geoscientific Model Development
Discussions
Open Access

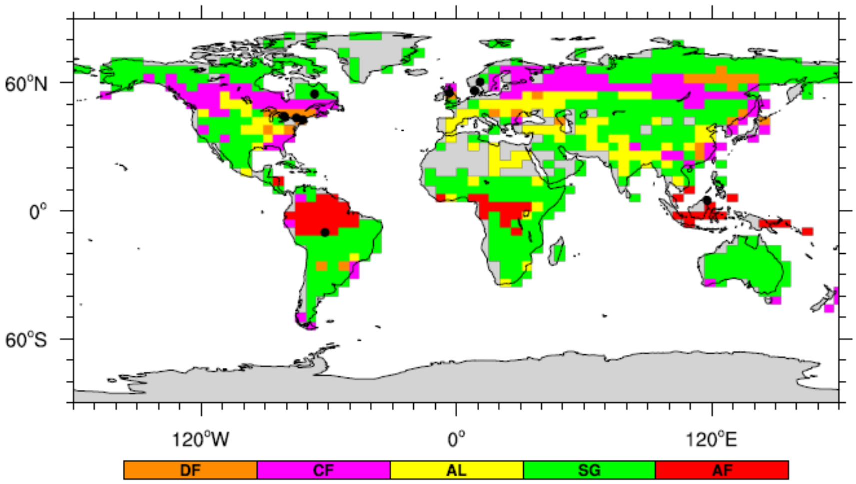

Figure 6 The major dry deposition type at each grid cell in GC model. Black dots indicate the locations of measurement sites used in evaluation (Table 2). DF, CF, AL, SG, AF represent deciduous forest, coniferous forest, agricultural land, shrub/grassland, and amazon forest, respectively.

https://doi.org/10.5194/gmd-2019-281
Preprint. Discussion started: 30 October 2019

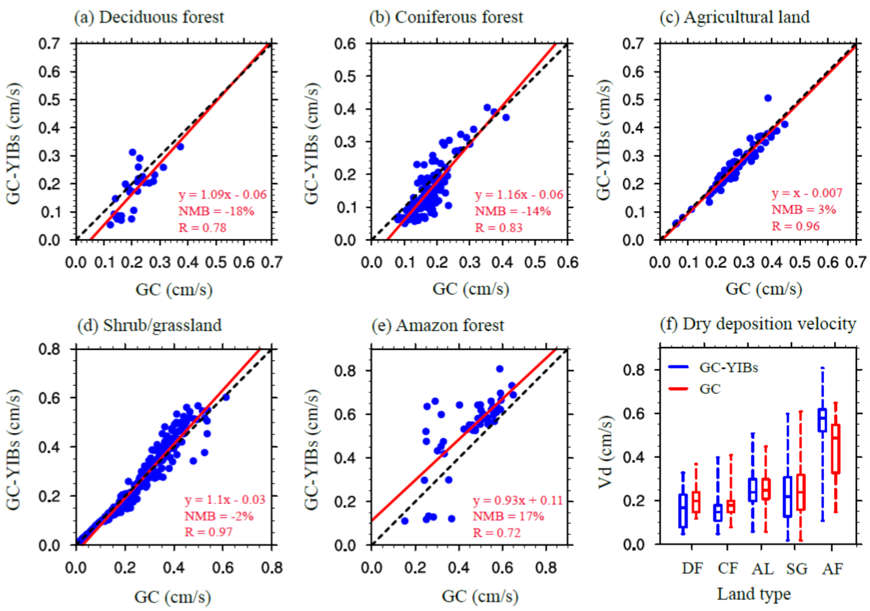

Figure 7 Comparisons of annual O_3 dry deposition velocity between online GC-YIBs and GC models for different land types, including (a) Deciduous forest, (b) Coniferous forest, (c) Agricultural land, (d) Shrub/grassland, and (e) Amazon forest. The box plots of dry deposition velocity simulated by online GC-YIBs (blue) and GC models (red) for different land types are shown in (f). Each point in (a)-(e) represents annual O_3 dry deposition velocity at one grid point averaged for period of 2010-2012. The red lines indicate linear regressions between predictions from GC-YIBs and GC models. The regression fit, correlation coefficient (R), and normalized mean biases (NMB) are shown on each panel.

https://doi.org/10.5194/gmd-2019-281
Preprint. Discussion started: 30 October 2019

Geoscientific Model Development
Discussions
Open Access

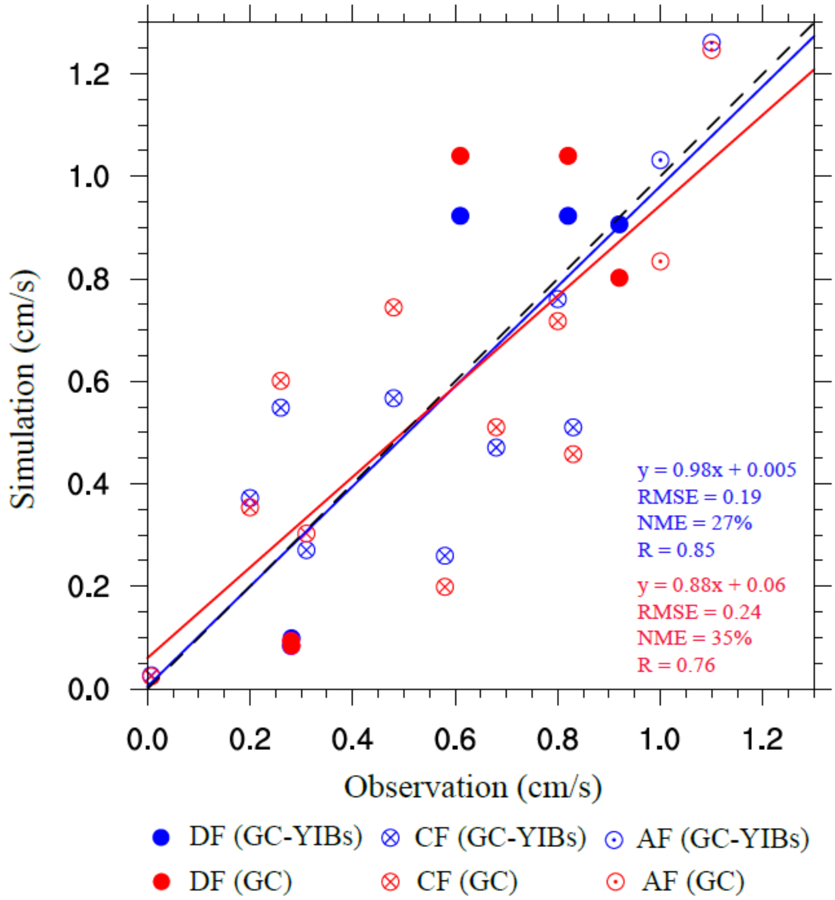

Figure 8 Comparison between observed and simulated O_3 dry deposition velocity at observational sites. The different marker types represent different land types. The blue and red markers represent the simulation results from online GC-YIBs and GC models, respectively. The blue and red lines indicate linear regressions between simulations and observations. The regression fits, root-mean-square errors (RMSE), normalized mean errors (NME) and correlation coefficients for GC-YIBs (blue) and GC (red) models are also shown.

Geoscientific Model Development
Discussions
Open Access

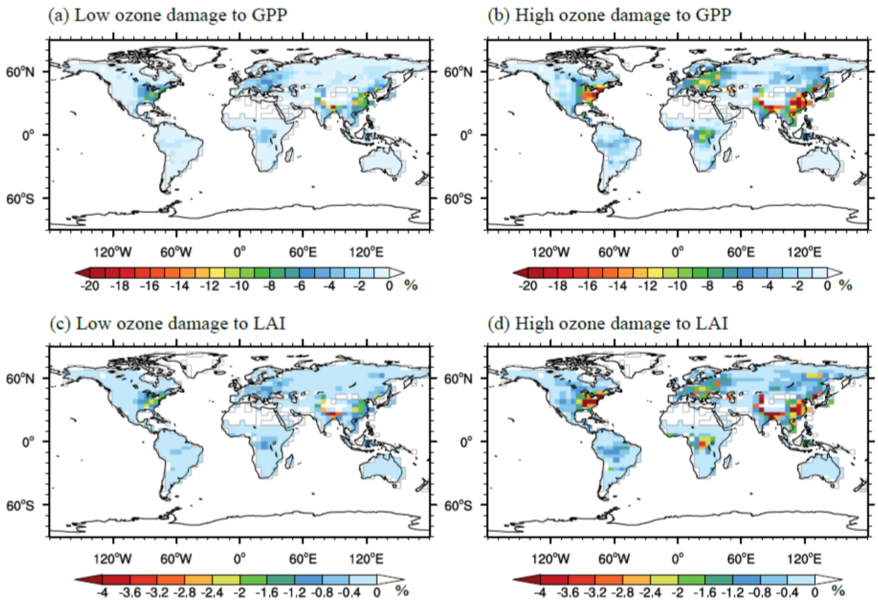

Figure 9 Percentage changes in (a, b) GPP and (c, d) LAI caused by O_3 damaging effects with (a, c) low and (b, d) high sensitivities. Both changes of GPP and LAI are averaged for 2010–2012.